

## Scattering of Magnetic Mirror Trapped Fast Electrons by a Shear Alfvén Wave

Yuhou Wang,<sup>1</sup> Walter Gekelman,<sup>1</sup> Patrick Pribyl,<sup>1</sup> and Konstantinos Papadopoulos<sup>2</sup>

<sup>1</sup>Department of Physics and Astronomy, University of California - Los Angeles, Los Angeles, California 90095, USA

<sup>2</sup>Department of Physics and Astronomy, University of Maryland, College Park, Maryland 20742, USA

(Received 19 October 2011; published 8 March 2012)

Laboratory observations of enhanced loss of fast electrons trapped in a magnetic mirror geometry irradiated by shear Alfvén waves (SAW) are reported. A population of runaway electrons generated by second harmonic electron-cyclotron-resonance heating, as evidenced by the production of hard x rays with energy up to 3 MeV, is subjected to SAW launched with a rotating magnetic field antenna. It is observed that the SAW dramatically affect the trapped fast electrons and scatter them out of the magnetic mirror despite any obvious resonance. The results could have implications on the techniques of artificial reduction of energetic electrons in the inner radiation belt.

DOI: 10.1103/PhysRevLett.108.105002

PACS numbers: 52.40.Db, 52.72.+v, 94.05.Pt

Wave-particle interactions play a key role in Earth's radiation belt formation, maintenance, and dynamics. The loss of the trapped charged particles and their evolution in phase space have been explained by various mechanisms involving naturally existing waves in space [1–3]. For field-aligned whistler waves ( $\omega \ll \Omega_e$ ) the dominant interaction is resonant pitch-angle scattering and precipitation of energetic electrons by naturally driven chorus and broadband hiss. Pitch-angle scattering can also occur by *L*-mode electromagnetic ion cyclotron waves (EMIC) with a frequency below the cyclotron frequency of the dominant species in multi-ionic plasmas. Both interactions have been considered as causing microbursts of precipitating MeV electrons [4–7]. Magnetosonic waves (also known as compressional Alfvén waves) can accelerate electrons to relativistic energies through the Landau resonance [8,9] or pitch-angle scatter them via oblique wave gyro-resonance [7]. Ultralow frequency (ULF) oscillations can accelerate electrons or protons via drift-resonant interactions [10,11]. The  $E_{\parallel}$  component of obliquely propagating kinetic Alfvén waves can lead to electron acceleration in the parallel direction [12–14].

Natural processes, such as Megastorms [15] as well as accidental or deliberate high altitude nuclear explosions can also lead to the enhancement of the MeV electron flux trapped in the inner radiation belt by several orders of magnitude, leading to catastrophic failure of the Low Earth Orbiting (LEO) satellites [16]. A 1962 exoatmospheric nuclear test ("Starfish Prime") produced an artificial radiation belt with an intense electron flux, and it took almost 10 years before the natural dynamic equilibrium of the radiation belts was restored [17]. Because the trapped energetic charged particles from such events pose severe hazards to expensive space satellites, there is a great deal of current interest in concepts that can lead to artificial remediation of the energetic trapped particles [18]. One example is enhancing electron precipitation by injecting whistler mode VLF waves in the inner radiation belt [19,20]. In

this Letter, we report the first clear demonstration of the scattering of energetic, magnetic mirror trapped electrons by shear Alfvén waves (SAW) in a lab experiment.

The experiment is performed on the Large Plasma Device (LaPD) [21] at the University of California, Los Angeles. A schematic of the experiment is shown in Fig. 1. The plasma is produced with a pulsed dc (direct current) discharge between a heated cathode and a mesh anode at one end of a stainless steel cylindrical vacuum chamber filled with  $2 \times 10^{-5}$  Torr helium gas. A confining static magnetic field is provided by solenoidal coils surrounding the vacuum chamber. The coils are divided into 10 sets along the  $z$  direction and driven by independently programmable power supplies. In this experiment, a symmetric magnetic mirror field centered at  $z = 0$  (10.75 m away from the cathode) is established, with  $B_{\min} = 437$  G and  $B_{\max} = 800$  G ( $R_{\text{mirror}} = 1.8$ ). The length of the mirror trap is 3.5 m measured between the two points where

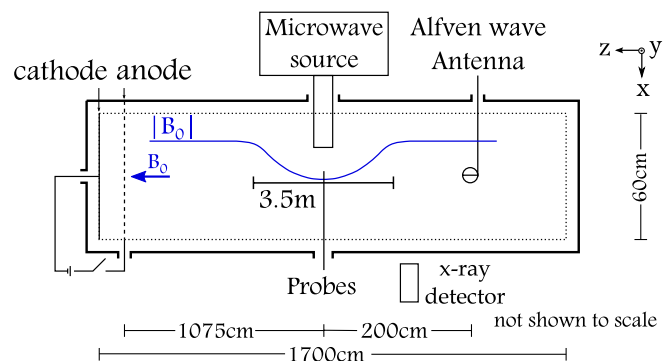


FIG. 1 (color online). Schematic of the experiment (not to scale). The cathode-anode separation is 0.55 m. The plasma column is 17 m long and 0.6 m in diameter. The magnetic coils are not shown. The center of the magnetic mirror defines the  $z = 0$  position. The length of mirror section is about 3.5 m. The Alfvén wave launcher is at  $z = -2.00$  m, and the cathode at  $z = 10.75$  m.

$B = 0.95B_{\max}$ . The experiment is done in the quiescent plasma after the dc discharge is switched off (plasma afterglow). The typical parameters for the background plasma are  $n_e \sim 5 \times 10^{11} \text{ cm}^{-3}$ ,  $T_e \sim 0.5 \text{ eV}$ , and  $T_i \leq T_e$ , length  $\sim 17 \text{ m}$ , and diameter  $\sim 0.6 \text{ m}$ . Movable probes inserted radially into the device provide diagnostics transverse to the magnetic field  $B_z$  ( $x$ - $y$  planes). The experiment is highly reproducible, and is repeated every second for weeks, allowing data collection over a set of spatial locations by moving only one probe with a computer controlled data acquisition system.

The background afterglow plasma is heated and a population of trapped fast electrons is generated by electron-cyclotron-resonance heating (ECRH). The microwave source used for heating is a 2.45 GHz magnetron, pulsed for 30–50 ms at a power up to 25 kW. The microwaves are introduced radially into the vacuum chamber through a 10 cm diameter cylindrical waveguide in the  $\text{TE}_{11}$  mode ( $E_{\text{microwave}} \parallel \hat{y}$ ). The end of the waveguide is 15 cm from the machine axis [Figs. 1 and 2(a)]. Different magnetic mirror field profiles were tested, and the ECR heating was found to be most efficient at  $f_{\text{microwave}} = 2f_{ce}$  at the field minimum. As observed in other experiments [22–26], the heated plasma consists of a thermalized warm plasma component as well as a population of runaway hot electrons. For the warm plasma  $T_e \sim 50 \text{ eV}$  and  $n_e \sim 3 \times 10^{11} \text{ cm}^{-3}$ , as measured by a Langmuir probe which was calibrated using a 60 GHz microwave interferometer.

X rays are generated by the hot electrons when they strike the machine wall or other metal objects in the chamber. They are detected by a NaI(Tl) scintillator detector located outside the vacuum chamber, with a solid angle span of  $0.004 \pm 0.002 \text{ sr}$  measured from the center of the magnetic mirror. The chamber wall is made of 3/8 inch thick stainless steel, which cuts off the x-ray transmission below  $\sim 100 \text{ keV}$ . Hot electrons with large pitch angles are trapped in the mirror field, and are continuously accelerated by the ECRH. These hot electrons drift in the azimuthal direction due to the grad- $B$  drift, forming a hot electron ring within the mirror trap. The ring shape is confirmed by (a) measurements of the density of the warm plasma component due to the microwave energized electrons ionizing neutral gas, and (b) a probe that blocks the path of hot electrons can completely eliminate x-ray production if inserted radially along the positive  $x$  axis or positive  $y$  axis [Fig. 2(a)]. The size and position of the hot electron ring is determined by inserting a “luminator probe” along the positive  $x$  axis. The probe consists of a 5 mm  $\times$  5 mm  $\times$  1 mm tungsten tip at the end of a ceramic rod [Fig. 2(b)]. The x-ray signal is intensified when the hot electrons strike the tungsten tip of the luminator, due to the high atomic number of the tungsten. The ceramic stalk does not have the same effect when it blocks the path of the hot electrons. Figure 2(b) shows the x-ray flux as a function of the tungsten tip position at different times after the start

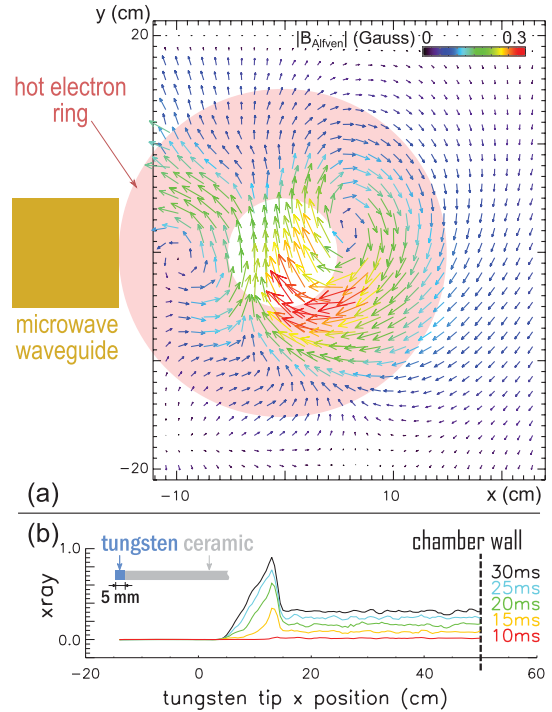


FIG. 2 (color). A plot of the plane at  $z = 0$ , showing the relative size and location of the microwave waveguide and the hot electron ring (the purple annulus). Also shown is a measurement of the Alfvén wave  $\vec{B}_\perp$  vectors on this plane 0.15 ms after the start of the Alfvén wave burst. (b) X-ray flux as a function of luminator probe tungsten tip position at different times during the ECRH. The probe is inserted radially along the positive  $x$  axis.

of the ECRH. The x-ray flux decreases to a negligible level when the ceramic stalk of the probe completely cuts through the ring. The ring thickness is measured to be 10 cm and remains constant after the ring is formed. The hot electron energies are determined to be in the range from 200 keV to 3 MeV using pulse height analysis of the x-ray signal.

SAW are launched by a rotating magnetic field (RMF) antenna [27,28], placed on the machine symmetry axis 2 m downstream from the center of the mirror section (Fig. 1). The antenna is composed of two orthogonal coils (placed in the  $x$ - $z$  and  $y$ - $z$  planes) with diameters of 8 and 9 cm. It is driven by two independent RF drivers with a  $\pi/2$  phase delay at  $f = 115 \text{ kHz}$ . The magnetic field of the Alfvén wave is measured with a 3-axis pickup loop. The measured  $\vec{B}_\perp$  vectors on the plane of  $z = 0$  at one instant in time are plotted in Fig. 2(a). The peak amplitude of  $B_{\text{wave}}$  measured at  $\Delta z = 2 \text{ m}$  is 0.5 Gauss ( $B_{\text{wave}}/B_0 < 0.2\%$ ). SAW have a magnetic field almost perpendicular to  $B_0$ , and electric field perpendicular to both  $B_0$  and  $B_{\text{wave}}$  [29]. The estimated  $E_{\text{wave}}$  amplitude to the first order is 0.5 V/cm [30], with  $E_{||}/E_{\perp} < 0.02$ .

Figure 3(a) shows the time series of x-ray flux measured after the ECRH turned on at  $t = 0$ . The black trace is

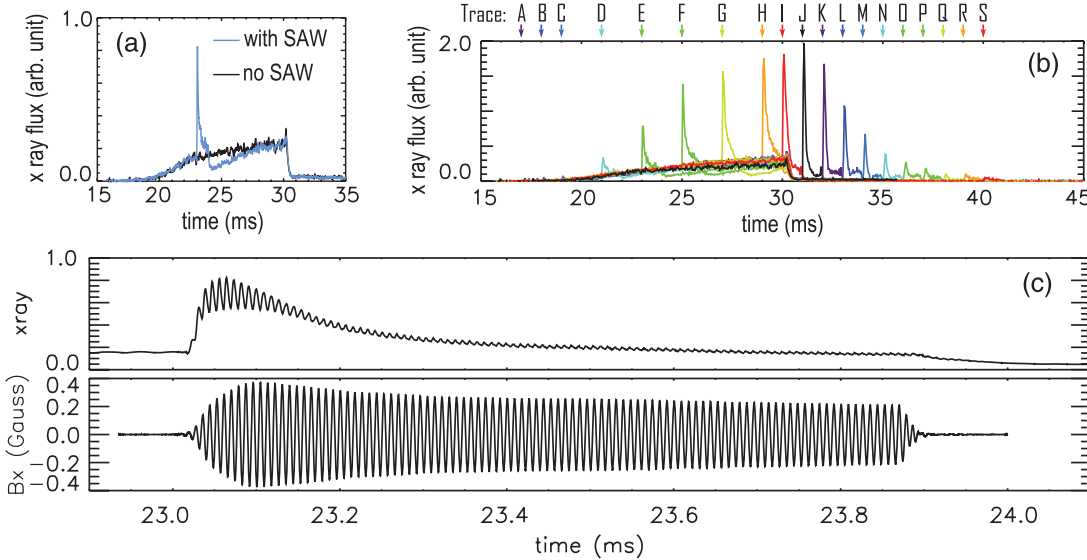


FIG. 3 (color). Time series of the x-ray flux. (a) Comparison of x-ray measurement with or without the presence of a 100-cycle SAW. The ECRH is on from  $t = 0$  to 30 ms, but only after about 20 ms are there sufficient high energy electrons to produce a measurable x-ray flux. (b) Overlay of 19 traces (designated A-S), each measured with a 100-cycle SAW launched at different time delays (marked by an arrow on the top). A population of fast electrons persists after the shutdown of the ECRH, and can be detrapped by application of the SAW to produce x-ray bursts. (c) 1200 shot averaged signal of the x-ray burst during SAW propagation.  $B_x$  of the SAW measured at the center of the magnetic mirror is shown on the bottom trace.

measured without launching an Alfvén wave. The more or less steady x-ray production comes from hot electrons which are slowly lost from the magnetic mirror and strike the chamber wall or other metallic objects. This is referred to as “the background x-ray production.” It is projected that the loss of electrons which gives rise to the background x rays is related to the presence of the microwaves, as evidenced by the fact that the background x-ray signal drops rapidly with the termination of the ECRH at  $t = 30$  ms.

The SAW is observed to effectively scatter the hot electron population. The blue trace in Fig. 3(a) is measured with a SAW burst 100 cycles long, launched at  $t = 23$  ms. A burst of x rays generated by hot electrons escaping the mirror trap appears during the Alfvén wave propagation time. A large flux of x rays appears while the Alfvén wave is first turned on. After this initial increase, during the rest of Alfvén wave propagation, the x-ray flux decreases as the hot electron population is depleted. After the Alfvén wave is turned off, the x-ray flux drops precipitously. Later in time ( $t > 24$  ms), the x-ray flux slowly builds up due to the presence of ECRH which is on for an additional 6 ms. Averaging over a large ensemble (1200 shots), the temporal history of the x-ray burst clearly shows a modulation at the frequency of the shear Alfvén wave as shown in Fig. 3(c).  $B_x$  of the Alfvén wave measured at the center of the mirror is shown for comparison.

Figure 3(b) shows an overlay of 19 traces. For each trace, a 100-cycle Alfvén wave is launched starting at a time between  $t = 17$  ms and  $t = 40$  ms. The starting time

of the Alfvén wave for each trace is marked by an arrow with the same color as the trace (designated A-S) on the top. At earlier times (traces A-C), the Alfvén wave does not have any impact on the x-ray flux, due to the low energy and density of the trapped electron population. In this series of experiments, it takes about 20 ms for a measurable background x-ray flux to be generated. We attribute this to the time it takes to accelerate a substantial electron population to energies that produce x rays measurable outside the 3/8 inch stainless steel vacuum chamber ( $> 0.1$  MeV). Loss of the low-energy electrons is not visible on the existing x-ray diagnostic. When the trapped electrons are further accelerated, characterized by the background x-ray production, the effect of Alfvén waves scattering trapped hot electrons described above appears (traces D-H). The runaway trapped electrons are present in the magnetic mirror after the ECRH terminates at  $t = 30$  ms. When the Alfvén wave is switched on at these late times the trapped electrons are scattered as evidenced in Fig. 3(b) traces J-S. This shows that detrapping is not affected by the presence of the microwaves. The estimated trapping time for a 1 MeV electron is 23 ms before its loss as a result of scattering from the atomic nucleus of the neutral helium gas atom. We observe hot electrons by Alfvén wave scattering for half of this time. The decay of the x-ray burst intensity after  $t = 31$  ms reflects the decay of the number of x ray producing hot electrons still in the mirror.

The scattering effect of Alfvén waves is also observed on electrons of lower energy ( $\sim 100$  eV, here referred to as

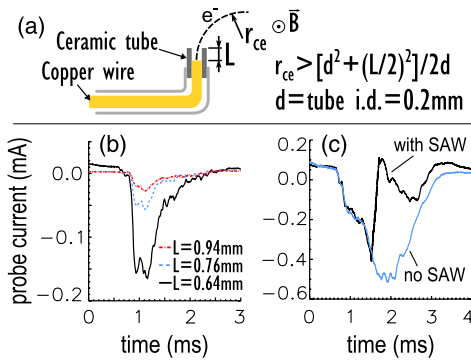


FIG. 4 (color online). (a) Schematic of the “soda-straw probe.” Electrons collected by this probe have gyroradii larger than a threshold value set by  $L$  (the distance the copper wire recessed into the ceramic tube) and  $d$  (ceramic tube inner diameter). (b) Current measured using soda-straw probe with 3 different recessed distances. The corresponding threshold energies are 140, 240, and 480 eV. The small positive signal at the outset of the  $L = 0.64$  mm trace is due to ions collected by the probe. (c) Comparison of cases with or without a SAW launched from  $t = 1.5$  ms to 1.7 ms.

“warm electrons”). In another series of experiments, the ECRH is injected for less than 3 ms with a power of 5 kW at a frequency near  $f_{ce}$ . In this case the magnetic mirror field is  $B_{\max} = 1200$  G and  $B_{\min} = 800$  G, and the SAW is launched for a duration of 0.2 ms. No x rays are observed. A “soda-straw probe” was developed to measure the trapped electron population with large  $v_{\perp}$ . The probe has a copper wire recessed into a 200  $\mu\text{m}$  diameter ceramic tube [Fig. 4(a)]. The copper wire is retractable with a micrometer with 1  $\mu\text{m}$  precision. The probe is situated in a plane perpendicular to  $B_0$  near the waveguide. Only electrons with gyro-radial larger than a threshold value, given in Fig. 4(a), could be collected on the copper wire and show up as negative current. Figure 4(b) shows 3 probe current traces measured with the collector wire recessed by different amounts. The ECRH is on from  $t = 0$  to 2 ms. At an early time before significant warm electrons are generated the signal from the background plasma is negligible compared to the electron current collected when warm electrons are present (see case  $L = 0.94$  mm). In the presence of warm electrons, the probe collects a negative current from electrons exceeding the threshold energy, and the probe current amplitude decreases with increasing  $L$  value. Based on this diagnostic, the measured warm electron perpendicular energy is  $\sim 10^2$  eV.

It is observed that the SAW also scatters these warm electrons. Figure 4(c) shows the soda-straw probe current (the probe is set to collect electrons with  $E_{\perp} > 80$  eV), comparing cases with or without launching Alfvén wave. The two traces overlap before the turn-on of the Alfvén wave at  $t = 1.5$  ms, showing a negative current from the warm electrons. In the black trace the warm electron signal rapidly decreases after the

Alfvén wave turns on, while in the blue trace the current remains negative without the wave. After the Alfvén wave is switched off at  $t = 1.7$  ms, the warm electron signal in the black trace slowly builds up due to the continuing ECRH.

The experimental results, especially the modulation of the loss rate at the SAW frequency are surprising and indicate that the injection of the shear Alfvén wave plays a catalytic role in controlling the bursts of precipitating energetic electrons as well as experiencing a feedback effect. Numerous radiation Belt observations show a strong correlation between the observed VLF waves (known also as hiss) excited by the anisotropy of trapped energetic electrons and simultaneous MHD oscillations. This is clearly seen by the deep periodic modulation in the intensity of the VLF noise and the precipitating electron fluxes that closely correlates with the observed magnetic pulsations, known as Pi-2 [31–33]. In fact Barfield and Coleman [34] demonstrated that the Pi-2 pulsations correspond to SAW over the entire field line. In this experiment the x-ray signal is modulated at the SAW frequency which suggests a similar mechanism. Either the presence of the SAW disturbs a situation of marginal stability [35] or directly scatters the electrons, which could bunch in phase space, by breaking one or more adiabatic invariants. These issues are currently under both theoretical and experimental investigation.

The authors thank Zoltan Lucky, Marvin Drandell, and Mio Nakamoto for their valuable technical support, and thank Jane Shin for probe testing. The authors also thank Dr. Shreekrishna Tripathi, Professor Liu Chen, and Professor George Morales for helpful discussions. We thank the referees for their useful comments. This work is supported by The Office of Naval Research and performed at the Basic Plasma Science Facility under ONR MURI 00014-07-1-0789. The BaPSF is funded by the Department of Energy and the National Science Foundation.

- 
- [1] R. Thorne, *Geophys. Res. Lett.* **37**, L22107 (2010).
  - [2] Y. Shprits, D. Subbotin, N. Meredith, and S. Elkington, *J. Atmos. Sol. Terr. Phys.* **70**, 1694 (2008).
  - [3] M. Schulz and L. Lanzerotti, *Particle Diffusion in the Radiation Belts* (Springer-Verlag, Berlin, 1974).
  - [4] T. O’Brien, M. Looper, and J. Blake, *Geophys. Res. Lett.* **31**, L04802 (2004).
  - [5] R. Thorne, T. O’Brien, Y. Shprits, D. Summers, and R. Horne, *J. Geophys. Res.* **110**, A09202 (2005).
  - [6] B. Ni and D. Summers, *Phys. Plasmas* **17**, 042902 (2010).
  - [7] B. Ni and D. Summers, *Phys. Plasmas* **17**, 042903 (2010).
  - [8] R. Horne, R. Thorne, S. Glauert, N. Meredith, D. Pokhotelov, and O. Santolik, *Geophys. Res. Lett.* **34**, L17107 (2007).

- [9] J. Bortnik and R. Thorne, *J. Geophys. Res.* **115**, A07213 (2010).
- [10] A. Chan, L. Chen, and R. White, *Geophys. Res. Lett.* **16**, 1133 (1989).
- [11] S. Elkington, M. Hudson, and A. Chan, *Geophys. Res. Lett.* **26**, 3273 (1999).
- [12] J. Wygant, A. Keiling, C. Cattell, R. Lysak, M. Temerin, F. Mozer, C. Kletzing, J. Scudder, V. Streltsov, and W. Lotko *et al.*, *J. Geophys. Res.* **107**, 1201 (2002).
- [13] C. Kletzing, *J. Geophys. Res.* **99**, 11095 (1994).
- [14] C. Hui and C. Seyler, *J. Geophys. Res.* **97**, 3953 (1992).
- [15] Y. Shprits, D. Subbotin, B. Ni, R. Horne, D. Baker, and P. Cruce, *Space Weather* **9**, S08007 (2011).
- [16] D. G. Dupont, *Sci. Am.* **290**, 100 (2004).
- [17] D. Beall, C. Bostrom, and D. Williams, *J. Geophys. Res.* **72**, 3403 (1967).
- [18] X. Shao, K. Papadopoulos, and A. Sharma, *J. Geophys. Res.* **114**, A07214 (2009).
- [19] U. Inan, T. Bell, J. Bortnik, and J. Albert, *J. Geophys. Res.* **108**, 1186 (2003).
- [20] J. Sauvaud, R. Maggiolo, C. Jacquey, M. Parrot, J. Berthelier, R. Gamble, and C. Rodger, *Geophys. Res. Lett.* **35**, L09101 (2008).
- [21] W. Gekelman, H. Pfister, Z. Lucky, J. Bamber, D. Leneman, and J. Maggs, *Rev. Sci. Instrum.* **62**, 2875 (1991).
- [22] H. Ikegami, H. Ikezi, M. Hosokawa, S. Tanaka, and K. Takayama, *Phys. Rev. Lett.* **19**, 778 (1967).
- [23] N. A. Uckan, *J. Fusion Energy* **1**, 49 (1981).
- [24] D. Smatlak, X. Chen, B. Lane, S. Hokin, and R. Post, *Phys. Rev. Lett.* **58**, 1853 (1987).
- [25] H. P. Warren and M. E. Mauel, *Phys. Rev. Lett.* **74**, 1351 (1995).
- [26] T. Simonen, *Proc. IEEE* **69**, 935 (1981).
- [27] A. Gigliotti, W. Gekelman, P. Pribyl, S. Vincena, A. Karavaev, X. Shao, A. Sharma, and D. Papadopoulos, *Phys. Plasmas* **16**, 092106 (2009).
- [28] A. Karavaev, N. Gumerov, K. Papadopoulos, X. Shao, A. Sharma, W. Gekelman, Y. Wang, B. Van Compernolle, P. Pribyl, and S. Vincena, *Phys. Plasmas* **18**, 032113 (2011).
- [29] W. Gekelman, S. Vincena, D. Leneman, and J. Maggs, *J. Geophys. Res.* **102**, 7225 (1997).
- [30] N. Palmer, W. Gekelman, and S. Vincena, *Phys. Plasmas* **12**, 072102 (2005).
- [31] N. Sato, K. Hayashi, S. Kokubun, T. Oguti, and H. Fukunisi, *J. Atmos. Terr. Phys.* **36**, 1515 (1974).
- [32] G. I. Korotova, N. G. Kleymenova, and O. M. Raspopov, *Geomagn. Aeron.* **15**, 149 (1975).
- [33] F. V. Coroniti and C. F. Kennel, *J. Geophys. Res.* **75**, 1279 (1970).
- [34] I. N. Barfield and P. J. Coleman, *J. Geophys. Res.* **75**, 1943 (1970).
- [35] A. V. Vodop'yanov, S. V. Golubev, A. G. Demekhov, V. G. Zorin, D. A. Mansfel'd, S. V. Razin, and V. Y. Trakhtengerts, *Plasma Phys. Rep.* **31**, 927 (2005).